scientific reports

Check for updates

OPEN

Integrated geochemical and geophysical assessment for monitoring soil stabilization with waste oyster shells

Sunjae Lee[1,2], Minju Kim[1,3], Narae Lee[1,4], Yongtae Ahn[5] & Jaeyoung Choi[1]✉

We assessed the field-scale stabilization efficiency of lead (Pb) and copper (Cu) in contaminated soils using powdered (WOS-P) and granular (WOS-G) waste oyster shell (WOS) amendments. A 9-month monitoring was conducted using geochemical leaching tests Toxicity Characteristic Leaching Procedure (TCLP), Mehlich-3, and Diethylenetriaminepentaacetic acid (DTPA) besides sequential extraction and geophysical methods. WOS-treated soils exhibited significant reductions in leaching ratios, with WOS-P showing greater efficacy. Pb and Cu leaching ratios decreased by up to 1.21 and 2.00% points, respectively. Fractional analysis confirmed the redistribution of Pb into carbonate-bound forms, with the F2 fraction increasing from 6.46 to 12.89%, and Cu into Fe–Mn oxide-bound forms (F3), which increased from 11.29 to 15.88%. Electrical resistivity (ER) and induced polarization (IP) surveys visualized the spatial evolution of stabilization. In WOS-P plots, lower ER and elevated IP responses were initially observed, consistent with those of increased ionic strength. Over time, signal attenuation suggested precipitation and geochemical fixation. WOS-G plots showed delayed IP enhancement, reflecting slower dissolution and ion release. Our results suggest that WOS can serve as an effective and sustainable stabilizer, and that combined ER and IP with geochemical monitoring offers valuable complementary insights. Future work should expand the spatial and temporal scope to validate these findings and advance integrated interpretation frameworks for more robust field applicability and quantitative stabilization assessment.

Keywords Soil stabilization, Heavy metal immobilization, Waste oyster shell (WOS), Geophysical monitoring, Chemical extraction method

Soil contamination by heavy metals such as lead (Pb) and copper (Cu) has become a global environmental concern due to their persistence, toxicity, and bio-accumulative properties. These contaminants originate from a variety of anthropogenic activities, including industrial emissions, mining, agricultural chemical use, and the uncontrolled disposal of solid waste[1]. Once released, heavy metals accumulate in soils over time, posing risks to terrestrial ecosystems and human health via plant uptake and trophic transfer, including carcinogenicity and neurotoxicity[2,3].

To mitigate these risks, numerous remediation technologies were developed, including biological, physical, and chemical methods. Among these, solidification/stabilization (S/S) gained significant attention as a practical and cost-effective strategy for immobilizing heavy metals in situ. The S/S process involves converting mobile and bioavailable metal species into chemically stable and less soluble forms through the addition of binding agents, thereby reducing leachability and environmental hazards[4,5]. Due to its reliability and scalability, the United States Environmental Protection Agency (US EPA) recognizes S/S as one of the most effective techniques for the management of hazardous wastes[6,7].

Conventional S/S binders include lime, Portland cement, phosphates, and geopolymer-based materials[8,9]. While these demonstrated varying degrees of success in reducing metal mobility, concerns related to

[1]Center for Climate and Carbon Cycle Research, Korea Institute of Science and Technology, Seoul 02792, Republic of Korea. [2]Graduate School of Energy and Environmental Policy, Korea University, Seoul 02841, Republic of Korea. [3]Department of Earth Resources and Environmental Engineering, Hanyang University, Seoul 04763, Republic of Korea. [4]Department of Earth and Environmental Sciences, Korea University, Seoul 02841, Republic of Korea. [5]Department of Civil & Energy System Engineering, Kyonggi University, Suwon 16227, Republic of Korea. ✉email: Jchoi@kist.re.kr

sustainability, cost, and environmental burden have increased interest in alternative, eco-friendly amendments derived from waste resources[9,10]. Waste oyster shells (WOS), primarily composed of calcium carbonate ($CaCO_3$), represent a promising material for S/S applications. Their inherent alkalinity can elevate soil pH, facilitating the precipitation of heavy metals as hydroxides or carbonates (e.g., $Pb(OH)_2$, $PbCO_3$, $Cu(OH)_2$), and reducing their solubility and toxicity[11,12].

In South Korea, the increasing volume of discarded oyster shells prompted regulatory actions, including the 2021 amendment to the Marine Waste and Marine Sediment Management Act (Act No. 18065), which promotes the reuse of marine biowaste[13]. This policy shift provides a practical and legal foundation for the valorization of WOS as a stabilizing agent in environmental remediation efforts.

Although the laboratory-scale mechanisms of WOS-mediated stabilization were well documented, comprehensive field-level evaluations particularly those integrating chemical fractionation with spatially resolved monitoring tools remain limited[14–16]. Most prior studies rely primarily on leaching assays such as the Toxicity Characteristic Leaching Procedure (TCLP) and Synthetic Precipitation Leaching Procedure (SPLP), which provide useful but limited insight into speciation dynamics and spatial heterogeneity within treated soils[17,18]. Therefore, a multi-method assessment framework is essential.

Sequential extraction protocols (e.g., Tessier method) enable detailed analysis of heavy metal redistribution among operationally defined fractions (exchangeable, carbonate-bound, Fe/Mn oxide-bound, etc.), while DTPA and Mehlich-3 extractions offer complementary information on metal bioavailability[19,20]. However, such chemical methods are inherently destructive and lack the capacity to characterize the broader physical properties of the treated zones[15].

Accordingly, electrical resistivity (ER) and induced polarization (IP) surveys can serve as powerful, non-invasive tools for evaluating S/S effectiveness in situ[21]. ER measurements are sensitive to changes in soil porosity, ionic strength, and water content, all of which are influenced by amendment-induced reactions. In contrast, IP responds to interfacial polarization phenomena caused by mineral precipitation, ion adsorption, and changes in surface conductivity[21–23]. These techniques provide real-time, spatially continuous data complementing chemical analyses, enabling the detection of physicochemical transformations and amendment transport behavior across the treated profile.

We aim to evaluate the effectiveness of powdered and granular WOS as stabilizing agents for Pb- and Cu-contaminated soils, using a comprehensive monitoring framework including leaching tests (TCLP, SPLP), chemical extractions (Mehlich-3, DTPA), sequential extraction (Tessier method), and geophysical methods (ER/IP). By integrating chemical and geophysical perspectives, we seek to elucidate both the immobilization mechanisms and the spatial-temporal evolution of amended soils, contributing to the development of field-applicable, sustainable S/S strategies based on waste-derived materials.

Materials and methods

Site characterization and pilot plot design

The selected study site is a former military shooting range located in Gwangam-dong, Dongducheon-si, Republic of Korea (Fig. 1a). The site has a history of extensive shooting activities, which have led to the accumulation of heavy metals, particularly lead (Pb) and copper (Cu), in the surface soils. According to preliminary soil analyses, the maximum Cu concentration was 441.56 mg/kg, which remained below the national warning standard. Contrastingly, Pb concentrations reached as high as 1,938.0 mg/kg, exceeding the Korean soil contamination warning threshold[24]. This exceedance indicated a potential environmental risk, justifying the selection of this location for the installation of pilot-scale stabilization plots. The groundwater table at the site was observed at depths ranging from 1.2 to 1.5 m below ground level.

Three pilot-scale test plots were constructed to evaluate the performance of the stabilizing agents, consisting of (i) a control plot containing only contaminated soil, (ii) a plot amended with powdered stabilizer, and (iii) a plot amended with granular stabilizer (Fig. 1b and c). Each plot measured 3 m × 3 m × 1 m, yielding a volume of 9 m^3, and was confined using 2 cm-thick waterproof plywood walls to prevent lateral mixing. The total volume of all three plots was 27 m^3.

In the amended plots, contaminated soil was first filled to a depth of 0.7 m. Then, a pre-mixed layer composed of contaminated soil and stabilizer (5% by weight) was placed over the top 0.3 m. This corresponds to 2.295 tons of contaminated soil mixed with 0.115 tons of stabilizing agent per treated plot. All plots were designed to achieve a target bulk density of 1.7 ton/m^3.

The physicochemical properties of the contaminated soil, WOS-P amended soil, and WOS-G amended soil after plot construction are summarized in Table 1. Soil texture was determined using the hydrometer method according to the USDA classification system. Soil pH was measured in a 1:5 (w/v) suspension with deionized water using a glass electrode pH meter. EC was analyzed in the same suspension using a conductivity meter (Thermo Scientific Orion Star A212). Cation Exchange Capacity (CEC) was determined by 1 M ammonium acetate (pH 7.0) saturation-exchange extraction followed by quantification using Kjeldahl distillation. TOC was measured via the Walkley–Black dichromate oxidation method. All measurements were conducted in triplicate, and results were expressed as means with standard deviations in parentheses.

Preparation and characterization of stabilizing agents

WOS used here were collected from a seafood market located in Tongyeong, South Korea. The WOS were subjected to a two-step washing process, initially rinsed with tap water to remove coarse impurities, followed by a second rinse with distilled water for finer purification. Subsequently, the shells were thermally treated in a single unit (SC ENG, S-IOV2250) first heated at 95 °C for 8 h, and then continuously dried at 105 °C for 72 h to eliminate residual moisture.

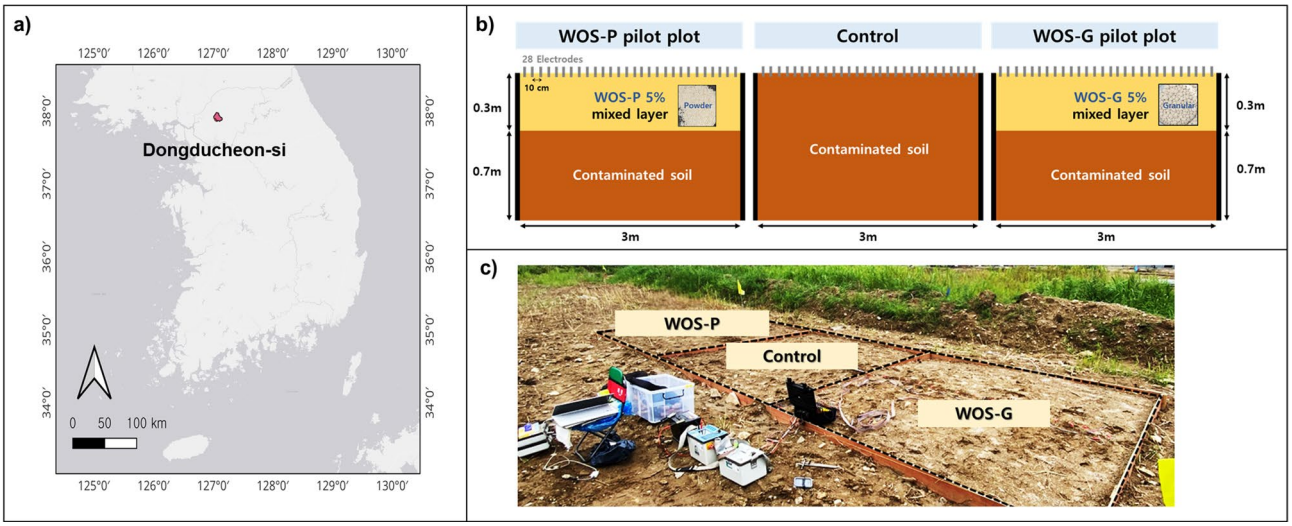

Fig. 1. Study site location and pilot plot design schematic. (a) Map showing the location of the experimental field site in Dongducheon-si, Gyeonggi Province, Republic of Korea (coordinates: 37.9034°N, 127.0605°E). (b) Cross-sectional diagrams of the three test plots (Testbed A, Control, Testbed B), each measuring 3 m × 3 m × 1 m, illustrating distribution of the stabilization layer (top 0.3 m, 5% WOS mixed) and underlying contaminated soil (0.7 m). Electrode positions and plot boundaries are indicated. (c) Field photograph showing the surface layout and physical boundaries of the test plots during initial setup. The map was created using QGIS version 3.43.3 (a free and open-source geographic information system, available at https://qgis.org). The basemap was sourced from OpenStreetMap (© OpenStreetMap contributors) via the QuickMapServices plugin. OpenStreetMap is open data, licensed under the Open Data Commons Open Database License (ODbL) by the OpenStreetMap Foundation (OSMF).

	Control Soil	WOS-*P* Soil	WOS-G Soil
Sand (%)	80.6 (1.26)	82.0 (1.02)	80.8 (2.09)
Silt (%)	13.4 (0.37)	12.0 (0.73)	12.7 (0.53)
Clay (%)	6.0 (0.91)	5.9 (0.25)	6.5 (0.11)
Texture	Sandy Loam	Sandy Loam	Sandy Loam
pH	5.26 (0.09)	7.22 (0.11)	7.29 (0.07)
EC (μS/cm)	730 (10.23)	3,980 (78.32)	2,380 (24.26)
CEC (Cmol/kg)	80.70 (1.13)	83.20 (1.68)	78.34 (5.35)
TOC (%)	3.14 (0.03)	5.03 (0.04)	4.15 (0.19)

Table 1. Physicochemical properties of contaminated soil and soils amended with WOS-P and WOS-G. Values in parentheses represent standard deviation ($n = 3$).

A two-stage crushing process was employed to achieve the desired particle size. First, a hammer crusher was used to reduce the WOS to particles smaller than 2 mm. This was followed by fine grinding with a ball mill crusher, yielding uniformly sized particles ranging from 100 to 1000 μm. However, the powdered form posed handling challenges during field application due to airborne dust generation. Therefore, the powder was mixed with distilled water in a 1:1 ratio to produce a slurry form that was more manageable for incorporation into the test plots.

The hammer and ball mill crushers were constructed from SS400 and S45C steel, materials known for their high resistance to corrosion and wear, ensuring stable operation and minimal material degradation during the crushing process.

For the granular form of the stabilizing agent, the WOS were subjected to a process involving input, mixing, and kneading (PM Tech, PT150UL), granulation (PM Tech, PT6025B), and drying (SC ENG, S-IOV2250). During the mixing and kneading stage, environmentally friendly flour and distilled water were added as binder components to facilitate granulation.

To characterize the mineralogical, elemental, and surface physicochemical properties of the WOS, a series of instrumental analyses was conducted. X-ray diffraction (XRD) analysis was performed using a Bruker D2 Phaser diffractometer with Cu-Kα radiation ($\lambda = 1.5406$ Å) to determine the crystalline phases. Elemental composition was assessed via X-ray fluorescence (XRF) spectroscopy using a Rigaku ZSX Primus II spectrometer. Fourier-transform infrared spectroscopy (FT-IR) was conducted using a PerkinElmer Frontier spectrometer over a wavelength range of 4000–400 cm^{-1} to identify functional groups.

Chemical evaluation of stabilized soils

Soil samples collected from each experimental plot were analyzed for Pb and Cu concentrations and speciation using six distinct methods. Total metal contents were determined via aqua regia digestion following ISO 11466, with quantification by inductively coupled plasma optical emission spectrometry (ICP-OES; Agilent Technology, 730 Axial). Leachability was evaluated using the toxicity characteristic (TCLP; EPA Method 1311) and the synthetic precipitation (SPLP; EPA Method 1312) leaching procedures, both involving agitation of 5.0 g of soil with respective extraction fluids for 18 h at 30 ± 2 °C, followed by filtration and ICP-OES analysis. Plant-available fractions of Pb and Cu were assessed using Mehlich-3 (0.2 M CH_3COOH + 0.25 M NH_4NO_3 + 0.015 M NH_4F + 0.013 M HNO_3 + 0.001 M EDTA, pH 2.5) and DTPA (0.005 M DTPA + 0.01 M $CaCl_2$ + 0.1 M triethanolamine, pH 7.3) extractions. For operationally defined speciation, the five-step Tessier sequential extraction procedure was employed to fractionate Pb and Cu into exchangeable, carbonate-bound, Fe/Mn oxide-bound, organic-bound, and residual forms. All analyses were conducted at two specific time points. The first was immediately following plot construction, and the second was after a 9-month field exposure period. Quality control was ensured by calibrating the ICP-OES instrument using a multi-point standard curve prepared from high-purity ICP multi-element standard solution IV (Certipur®, Sigma-Aldrich, product number 1.11355), achieving a correlation coefficient (R^2) of ≥ 0.9999 prior to sample analysis. Procedural blanks and duplicate samples were included in each analytical batch to monitor potential contamination and assess method precision. All extractions and ICP-OES measurements were conducted in triplicate, and relative standard deviations (RSDs) for replicate measurements were maintained below 5%.

Geophysical assessment of stabilized soils

ER and IP surveys were conducted at the same time points as the soil sampling, immediately following plot construction and after a 9-month field incubation. Measurements were performed using a Syscal Pro resistivity/IP system (IRIS Instruments, France). A dipole–dipole array configuration was employed with 28 electrodes spaced at 10 cm intervals along a linear transect. To minimize electrode-induced polarization effects, all measurements were conducted using high-purity silver electrodes (≥ 99% purity), which were inserted to a shallow depth (~ 2 cm) to ensure consistent ground contact. A constant injection voltage of 800 V was applied, and IP time-domain responses were integrated over a 1,000 ms window. Any reading with a standard error exceeding 5% was remeasured at least twice and up to four times to meet the reliability threshold. The resulting apparent resistivity and chargeability data were inverted using DC2d software to generate two-dimensional subsurface profiles. RMS misfit values were used as the primary criterion for inversion quality assessment.

Results and discussion

Characteristics of the stabilizing agent and treated soils

To understand the fundamental properties of the WOS amendment and its potential to alter the soil environment, we first characterized its key physicochemical and mineralogical features (Fig. 2). This initial analysis is crucial for hypothesizing the primary stabilization mechanisms that will be investigated later.

Figure 2 presents the physical forms and compositional characteristics of the WOS materials in both powder and granular forms, as examined by photographic documentation, FT-IR spectroscopy, X-ray diffraction (XRD), and X-ray fluorescence (XRF). The FT-IR spectra of the WOS samples (Fig. 2b) exhibited characteristic absorption bands of calcite ($CaCO_3$). A broad peak at 3444 cm^{-1} was assigned to O–H stretching vibrations associated with adsorbed moisture or hydroxyl groups. Weak bands at 2929 and 2521 cm^{-1} correspond to C–H stretching and possible bicarbonate-related vibrations. The intense bands at 1416, 879, and 709 cm^{-1} are diagnostic of calcite, representing asymmetric stretching, out-of-plane bending, and in-plane bending modes of the carbonate group, respectively. These spectral features confirm that the WOS material is predominantly composed of calcite, with only minor contributions from moisture or organic residues, and are consistent with the mineralogical composition identified by XRD analysis (Fig. 2c).

XRD pattern of the WOS confirmed that calcite ($CaCO_3$) was the dominant crystalline phase (Fig. 2c). All major peaks corresponded to the standard diffraction pattern of calcite, with sharp and intense peaks observed at 2θ values around 29.4°, 39.4°, 43.1°, 47.5°, and 48.5°, indicating the high crystallinity of the material. No secondary crystalline phases such as aragonite or dolomite were detected, suggesting a homogeneous calcite composition.

XRF analysis further supported these results by showing that CaO and CO_2 accounted for approximately 41.00% and 45.90% of the total mass, respectively (Fig. 2d), which corresponds well to those of the theoretical composition of pure calcite. Minor oxides such as B_2O_3 (7.50%), Na_2O (0.97%), SO_3 (0.76%), and trace elements including MgO, SiO_2, and Al_2O_3 were also present, although in concentrations below 1%. These impurities are likely derived from biological and environmental deposition on the shell surface during oyster growth and are not expected to significantly affect the calcite-dominated geochemical reactivity.

The high CaO content is particularly relevant to the heavy metal stabilization mechanism. Under alkaline conditions facilitated by the dissolution of $CaCO_3$, divalent metal cations such as Pb^{2+} and Cu^{2+} can precipitate as low-solubility carbonate forms (e.g., $PbCO_3$, $CuCO_3$), thereby reducing their leachability and bioavailability. Furthermore, the fine crystalline structure of calcite contributes to surface-controlled sorption and possible ion exchange processes that promote metal immobilization. However, environmental changes such as acidification and redox shifts can alter calcite stability and surface chemistry, potentially leading to the remobilization of stabilized metals over time. Therefore, while calcite can aid in long-term immobilization under stable conditions, its effectiveness may diminish under fluctuating environmental factors[25–27].

The incorporation of WOS, either in powdered or granular form, did not alter the soil texture class, which remained classified as Sandy Loam across all treatment groups. This indicates that the particle size distribution of the added material did not significantly shift the overall granulometric structure. However, prominent changes

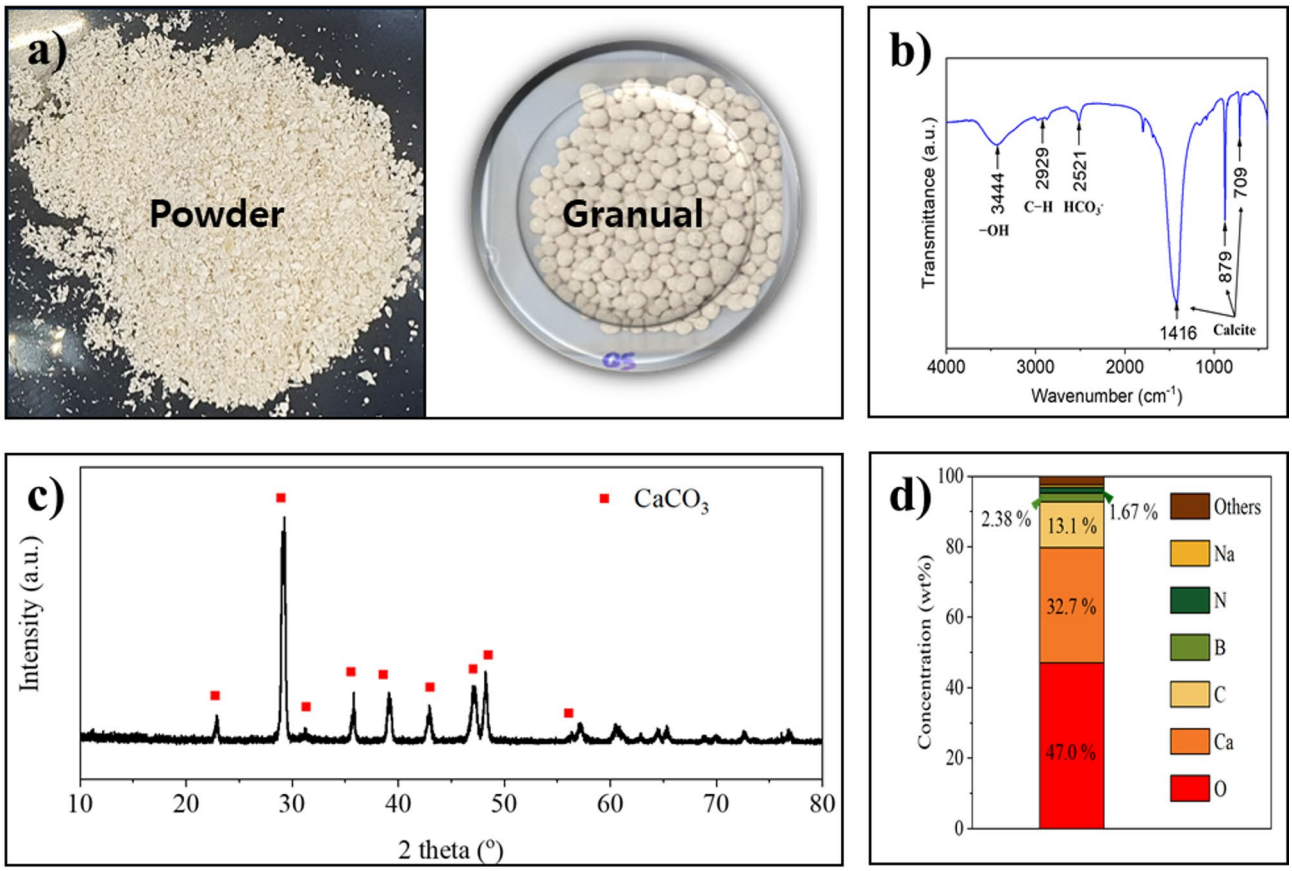

Fig. 2. Physical appearance and physicochemical characterization of the WOS stabilizing agent. (a) Photographs of WOS-P and WOS-G used for stabilization treatments. (b) FT-IR spectra identifying functional groups such as hydroxyl (-OH), organic matrix C–H, bicarbonate (HCO_3-), and carbonate minerals (notably calcite). (c) X-ray diffraction (XRD) pattern showing that calcite ($CaCO_3$) is the dominant crystalline phase. (d) X-ray fluorescence (XRF) analysis indicating that Ca (32.7%), O (47.0%), and C (13.1%) constitute the majority of the elemental composition of the WOS.

were observed in soil pH and EC. The pH increased from 5.3 in the contaminated soil to 7.22 and 7.29 in the powdered and granular WOS-amended soils, respectively. This pH elevation reflects the intrinsic alkaline nature of $CaCO_3$, the dominant phase in WOS, which readily dissociates under moist conditions to release OH^- and CO_3^{2-} ions. These reactions act as a buffering mechanism, neutralizing soil acidity.

EC values showed a pronounced increase following WOS amendment, with values rising from 730 µS/cm in the untreated soil to 3980 µS/cm and 2380 µS/cm in the WOS-P and WOS-G treatments, respectively. This suggests that the dissolution of ionizable components in WOS contributed to an elevated concentration of soluble salts in the pore water. The higher EC observed in the WOS-P treatment likely results from the increased surface area and finer particle size, which accelerates dissolution and ionic release compared with those of the more structurally intact WOS-G particles.

CEC values remained relatively stable across treatments, ranging from 783.42 to 831.97 cmol/kg, indicating that the addition of WOS did not significantly affect the capacity of the soil to retain exchangeable cations. This stability may be attributed to the dominance of quartz and sand-sized particles in the original soil matrix, as well as the limited contribution of $CaCO_3$ to permanent charge sites.

Contrastingly, TOC increased from 3.14% to 5.03% and 4.15% in the WOS-P and WOS-G treatments, respectively. This moderate increase may be partially explained by the inclusion of residual organic matrices or microbial biofilms associated with oyster shells, especially prior to thermal treatment. Additionally, the enhanced microbial activity at higher pH and Ca^{2+} concentrations could stimulate microbial turnover and necromass accumulation, indirectly contributing to TOC increases. This hypothesis aligns with reports suggesting that carbonate amendments can enhance microbial community stability and organic matter protection under near-neutral pH conditions.

Assessment of Pb and Cu leachability and speciation for long-term stability evaluation

To directly evaluate the stabilization efficiency of WOS (a primary objective of this study), we conducted a series of chemical leaching tests over a 9-month period. These tests were chosen to assess metal mobility from multiple perspectives. TCLP simulates environmental risk under landfill conditions, while DTPA and Mehlich-3 provide

an estimate of bioavailability (Figs. 3 and 4). Furthermore, to understand the specific geochemical mechanisms responsible for this stabilization, we employed the Tessier sequential extraction method (Fig. 5). This analysis is crucial as it reveals how the chemical forms, or speciation, of Pb and Cu shifted from more mobile to more stable fractions within the soil matrix, providing insight into how immobilization was achieved.

The total concentrations of Pb and Cu in the soils from each experimental plot were determined by aqua regia digestion and are summarized in Table 2. These baseline values, presented as mean and standard deviation, are essential for contextualizing the results from the TCLP, Mehlich-3, DTPA, and Tessier leaching tests.

Figure 3 presents the leaching behavior of Pb and Cu in soils sampled immediately after test plot construction, using three extraction methods of TCLP, Mehlich-3, and DTPA. Leaching was evaluated in terms of both (i) absolute leached concentrations (mg/kg) and (ii) leaching ratios expressed as a percentage of total metal content (% of total content). This dual representation provides complementary perspectives. While absolute concentrations offer direct comparability across treatments, leaching ratios allow normalization to account for differences in total metal content. Thus, interpretation based solely on absolute values can be misleading under varying background concentrations. SPLP results were excluded from analysis as all values fell below the detection limit (0.1 mg/L, ICP-OES).

Leaching concentrations (Fig. 3a and c) revealed that all WOS-treated soils (WOS-P and WOS-G) exhibited reduced extractable Pb and Cu levels compared with those of the untreated control.

Under TCLP, which simulates acidic leaching under landfill-like conditions, Pb concentration decreased from 12.40 mg/kg (control) to 10.88 mg/kg (WOS-P) and 9.64 mg/kg (WOS-G), corresponding to reductions of 1.52 and 2.76 mg/kg, respectively. Leaching ratios also declined from 1.28% (control) to 0.94% (WOS-P) and 0.93% (WOS-G), confirming that both forms of WOS effectively lowered environmentally relevant Pb mobility[28]. Cu followed a similar trend, with TCLP-extractable Cu declined from 2.58 mg/kg in the control to 2.10 mg/kg (WOS-P) and 2.23 mg/kg (WOS-G). This resulted in corresponding leaching ratio reductions of 0.29 and 0.26% points, respectively.

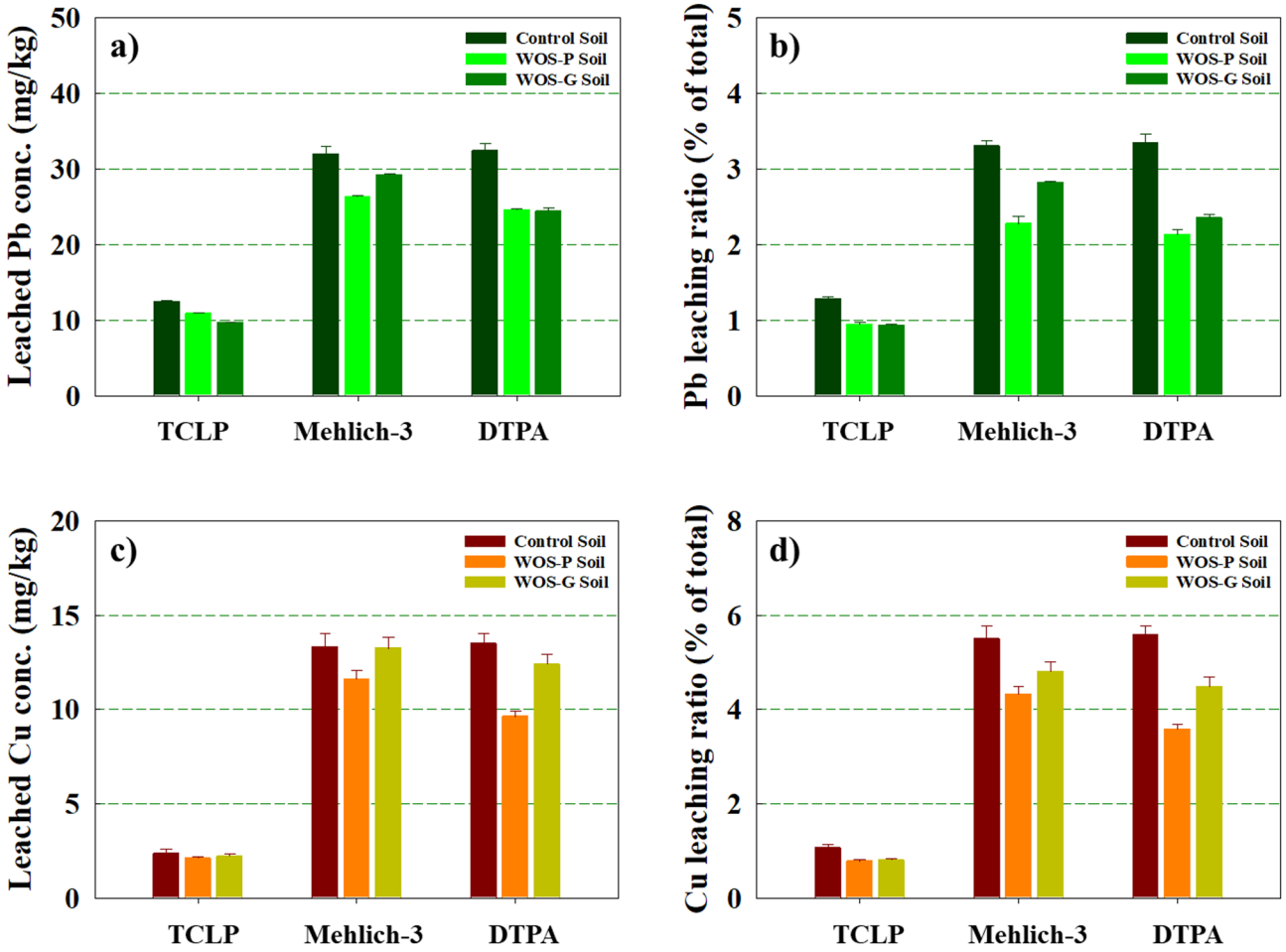

Fig. 3. Leaching concentrations and leaching ratios of Pb and Cu in soils immediately after test plot construction, including control soil and WOS-treated soils (WOS-P and WOS-G), using three extraction methods: TCLP, Mehlich-3, and DTPA. (a) Leached Pb concentration (mg/kg); (b) Pb leaching ratio (% of total content); (c) Leached Cu concentration (mg/kg); (d) Cu leaching ratio (% of total content). SPLP results are not presented as all values were below the instrumental detection limit of 0.1 mg/L for ICP-OES.

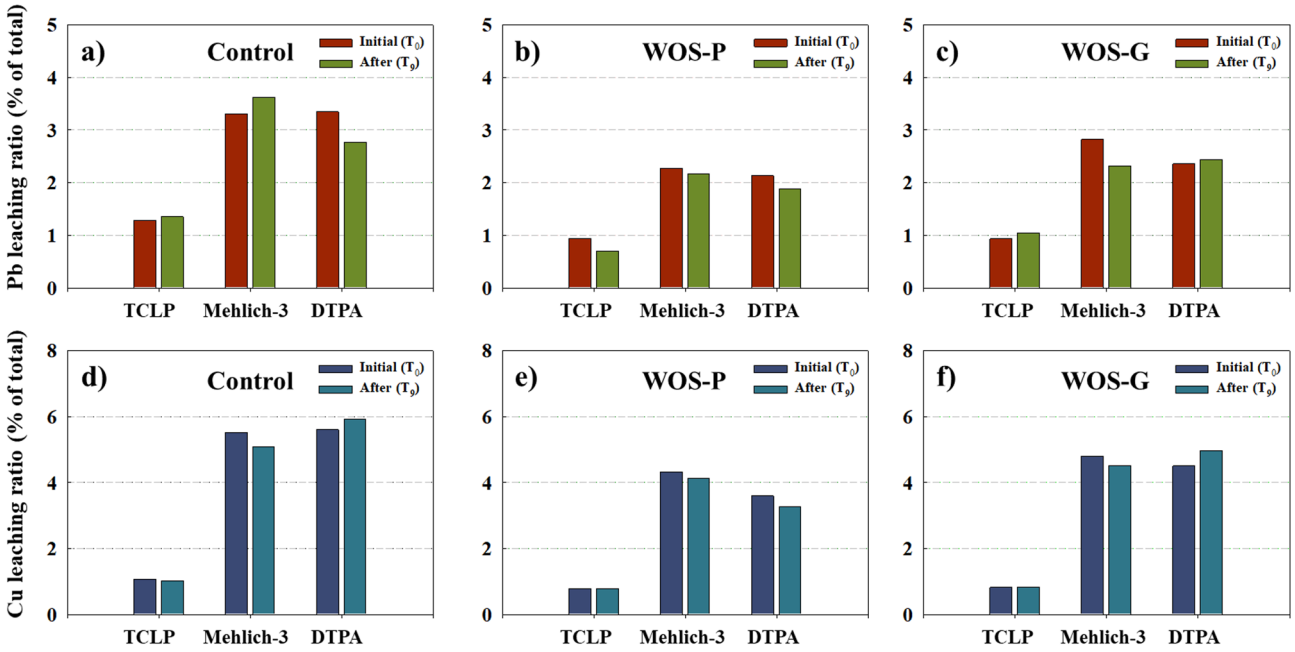

Fig. 4. Leaching ratios (% of total content) of Pb (a–c) and Cu (d–f) in soils sampled from three test plots Control (a, d), WOS-P (b, e), and WOS-G (c, f) based on three extraction methods: TCLP, Mehlich-3, and DTPA. The leaching ratio represents the proportion of each metal extracted relative to its total content. Each bar compares the results from soils sampled immediately after test plot construction (T_0) and after 9 months (T_9), thereby indicating the temporal stability or fluctuation of metal mobility following stabilization treatment.

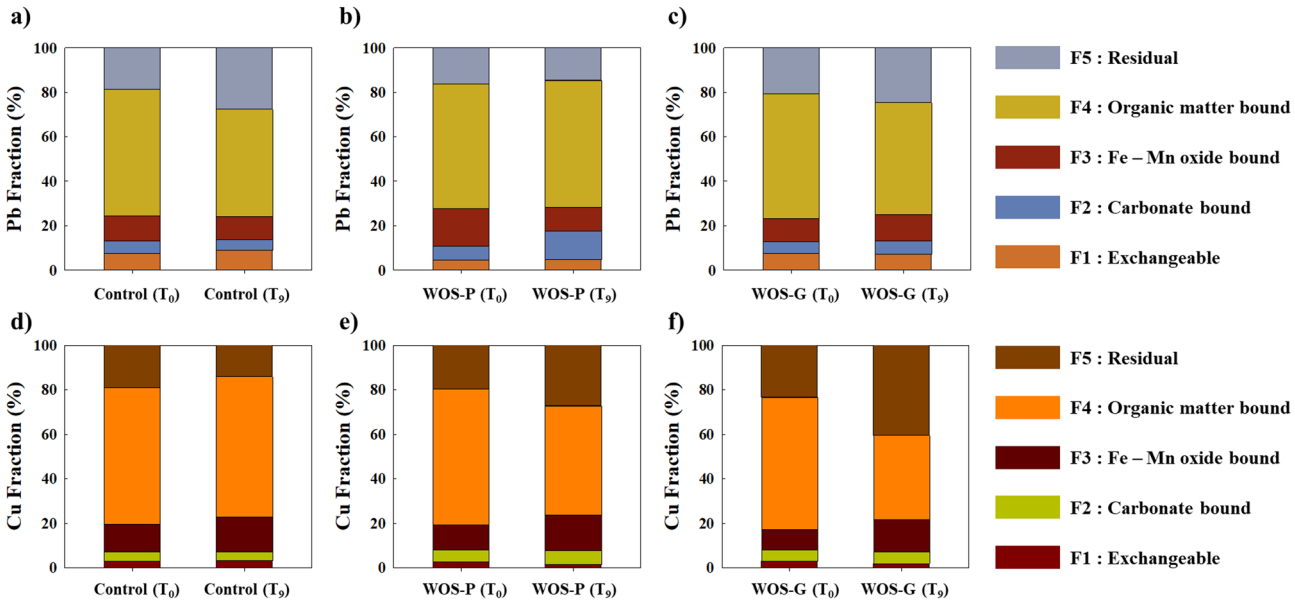

Fig. 5. Fractional distribution of Pb and Cu in soils based on the Tessier sequential extraction method before (T_0) and after 9 months (T_9) of stabilization. (a–c) Pb fraction distribution in control soil (a), WOS-P treated soil (b), and WOS-G treated soil (c). (d–f) Cu fraction distribution in control soil (d), WOS-P treated soil (e), and WOS-G treated soil (f).

In Mehlich-3, Pb concentrations were 31.99 mg/kg (control), 26.26 mg/kg (WOS-P), and 29.25 mg/kg (WOS-G). Corresponding leaching ratios declined from 3.30% to 2.27% and 2.82%, resulting in reductions of 1.03 and 0.48% points, respectively. For Cu, the control soil yielded 13.29 mg/kg, compared with that of 11.46 mg/kg (WOS-P) and 12.89 mg/kg (WOS-G), again indicating more effective stabilization in WOS-P. Mehlich-3 is a composite reagent of weak acids and chelating agents, enabling extraction of exchangeable, carbonate-

Element	Pilot plot	Initial (mg/kg)	After 9 months (mg/kg)
Pb	Control	968.97 (7.27)	783.83 (3.90)
	WOS-P	1154.49 (30.22)	1085.56 (7.41)
	WOS-G	1037.67 (3.91)	965.88 (6.08)
Cu	Control	241.73 (1.19)	258.00 (0.41)
	WOS-P	268.70 (0.84)	247.90 (0.95)
	WOS-G	275.92 (0.81)	268.55 (0.93)

Table 2. Total concentrations of Pb and Cu in soils from the Control, WOS-P, and WOS-G plots at the initial stage and after 9 months of field exposure. Values in parentheses represent standard deviation ($n = 3$).

bound, and Fe/Mn oxide-bound fractions (F1–F3)[29,30]. Its comparatively aggressive extraction capacity explains the higher absolute values compared with those of DTPA.

In DTPA, leached Pb concentrations were 32.38 mg/kg (control), 24.61 mg/kg (WOS-P), and 24.41 mg/kg (WOS-G). Although the absolute values for the two WOS treatments appeared similar, their normalized leaching ratios differed, with values of 3.34% (control), 2.13% (WOS-P), and 2.35% (WOS-G). This represented absolute reductions of 1.21 and 0.99% points, respectively. For Cu, DTPA-extractable concentrations declined from 13.50 mg/kg (control) to 9.64 mg/kg (WOS-P) and 12.38 mg/kg (WOS-G), while leaching ratios dropped from 5.59% to 3.59% and 4.49%, respectively. DTPA selectively targets metals in exchangeable and organically complexed forms (F1 and partial F4) under neutral pH conditions, resulting in generally lower extraction capacity than that of Mehlich-3[30,31].

Across all methods, WOS-P consistently outperformed WOS-G. This enhanced performance is likely due to its finer particle size, which increases surface area and enhances interaction with metal ions. The high $CaCO_3$ content of WOS promotes metal immobilization through precipitation (e.g., $PbCO_3$, $CuCO_3$), pH buffering, and ionic exchange reactions[16,32].

Summarily, WOS incorporation effectively reduced the mobility of Pb and Cu in all treated soils, with WOS-P demonstrating superior stabilization performance relative to that of WOS-G. Leaching concentrations and ratios consistently decreased across all extraction methods, affirming the efficacy of this waste-derived stabilizing agent. Furthermore, comparison among extraction methods highlighted that TCLP provides regulatory insight, Mehlich-3 captures a broader fraction of potentially mobile metals, and DTPA reflects bioavailable and weakly bound fractions. These complementary behaviors emphasize the importance of multi-method extraction strategies in field-scale stabilization assessment.

Figure 4a–f compares the leaching ratios (% of total content) of Pb (a–c) and Cu (d–f) from soils sampled at two time points immediately after test plot construction (T_0) and after 9 months (T_9) across three extraction methods (TCLP, Mehlich-3, and DTPA). Corresponding changes in the chemical speciation of Pb (Fig. 5a–c) and Cu (Fig. 5d–f), as determined by Tessier sequential extraction, were used to interpret the underlying mechanisms of metal immobilization.

In WOS-P soils (Fig. 4b and e), both Pb and Cu showed consistent reductions in leaching ratios across most extraction methods over the 9-month period. Under TCLP, Pb concentrations decreased from 0.94% to 0.70% (a reduction of 0.24% points). Similarly, concentrations under Mehlich-3 decreased from 2.27% to 2.16% (−0.11% points), and under DTPA, they decreased from 2.13% to 1.87% (−0.26% points). Compared with those of Pb, Cu exhibited higher leaching ratios across all extraction methods and also showed a more pronounced decrease over time. In WOS-P soils (Fig. 4e), Cu leaching ratios were prominently higher than those of Pb, particularly under Mehlich-3 and DTPA extractions. Over the 9-month period, Cu leaching declined from 4.32 to 4.11% (−0.21% points) for Mehlich-3 and from 3.59 to 3.26% (−0.33% points) for DTPA, while TCLP remained stable at 0.78%. These findings indicate that the stabilizing effect of the powdered WOS amendment was largely retained.

Contrastingly, WOS-G soils (Fig. 4c and f) displayed less stable patterns. Under TCLP, Pb leaching ratios decreased from 0.93% to 0.91%, and under Mehlich-3, they decreased from 2.82% to 2.38%. However, under DTPA, the ratios increased slightly from 2.35% to 2.48%. Cu results in WOS-G soils (Fig. 4f) were more variable compared with those in WOS-P. TCLP-based leaching ratios decreased slightly from 0.81 to 0.82% (+0.01% points), while Mehlich-3 showed a moderate reduction from 4.80 to 4.63% (−0.17% points). Contrastingly, DTPA-extractable Cu increased notably from 4.49 to 4.96% (+0.47), representing the largest change among all Cu extraction results. These observations suggest that, relative to WOS-P, the granular form of the amendment exhibited a less consistent and possibly less effective stabilization performance under field conditions.

The control soils (Fig. 4a and d), lacking any amendment, showed no stabilization. For Pb, leaching ratios increased under TCLP (from 1.28% to 1.35%) and Mehlich-3 (from 3.30% to 3.62%), but slightly decreased under DTPA (from 3.34% to 2.76%). For Cu, the trend was inconsistent: the leaching ratio decreased under Mehlich-3 (from 5.50% to 5.07%) but increased under DTPA (from 5.59% to 5.92%).

The Tessier sequential extraction analysis provides indirect chemical evidence that helps to elucidate the potential stabilization mechanisms at play (Fig. 5). To interpret these chemical extraction results, Fig. 5a–f illustrates the distribution of Pb and Cu across the five operationally defined fractions of the Tessier scheme. In the control soils (Fig. 5a and d), where no stabilizing agent was applied, the carbonate-bound fractions (F2) of both Pb and Cu remained relatively unchanged over the 9-month monitoring period 5.55–4.92% for Pb and 4.04–4.00% for Cu indicating the absence of a geochemical shift capable of promoting stable phase formation.

Contrastingly, WOS-P soils exhibited distinct speciation changes for both metals. For Pb (Fig. 5b), the F2 fraction nearly doubled, increasing from 6.46 to 12.89% at T_0 and T_9, respectively, suggesting the formation of sparingly soluble $PbCO_3$ (cerussite) under alkaline conditions. This transformation was likely driven by the $CaCO_3$-rich composition of the WOS, which increased soil pH and thereby facilitated the precipitation of carbonate-bound Pb phases[33]. This mechanism aligns with recent pilot-scale field research where carbonate-based amendments, such as half-burnt dolomite, were also found to effectively immobilize Pb via carbonate precipitation[34]. Cu speciation in WOS-P (Fig. 5e) showed a more complex trend. while the F2 increased slightly (5.35% to 6.32%), a more pronounced shift was observed in the Fe–Mn oxide-bound fraction (F3), which rose from 11.29 to 15.88%. This redistribution reflects increasing Cu association with redox-active oxide surfaces, particularly Fe and Mn oxides[35]. The crucial role of iron oxides in contaminant sequestration is well-documented, with recent long-term field studies confirming the high efficiency of iron-based adsorption layers in immobilizing metalloids[36,37].

The mechanism behind this Cu shift is likely due to the aging of the WOS amendment, which not only sustained elevated pH but also promoted the precipitation of hydrous ferric oxides (HFOs)[38]. These amorphous phases exhibit high surface area and strong affinity for divalent cations such as Cu^{2+}, enabling the progressive transfer of Cu from labile pools (F1–F2) to more stable oxide-bound forms (F3)[39]. This trend is consistent with earlier reports stating that Cu tends to preferentially sorb to Fe–Mn oxides, whereas Pb more readily precipitates as carbonates[40,41].

In the WOS-G treatment, speciation changes were present but generally less pronounced. For Pb (Fig. 5c), the carbonate-bound fraction increased from 5.28 to 5.99%, a smaller gain compared with that of WOS-P. Similarly, in Fig. 5f, Cu showed a slight F2 increase (5.01% → 5.22%) and a modest F3 increase (9.09% → 14.50%), indicating partial but weaker stabilization. These patterns align with those of the leaching results in Fig. 4c and f, where WOS-G showed smaller reductions in leaching ratios compared with those of WOS-P (Fig. 4b and e), especially under DTPA extraction for Cu.

Collectively, these results suggest that while both forms of WOS improved Pb and Cu immobilization, WOS-P demonstrated superior efficacy, as evidenced by the more substantial shifts from labile to stable fractions in Tessier extraction and the greater reductions in leaching ratios across multiple chemical extractions. The enhanced performance of WOS-P is likely attributable to its larger reactive surface area and higher dissolution rate, which promote more efficient interaction with soil contaminants and geochemical conversion pathways. The significance of particle size on geochemical reactivity is supported by other recent findings where finer particle fractions of materials were shown to be more critical in contaminant interactions[36].

Electrical resistivity and induced polarization monitoring of soil stabilization

To complement the point-based chemical analyses and to monitor the spatio-temporal evolution of the stabilized soil non-invasively, geophysical surveys were conducted (Fig. 6). Electrical resistivity is highly sensitive to changes in pore-water chemistry and soil structure, allowing us to visualize how the in-situ effects of the WOS amendment progressed across the entire test plot over time.

Figure 6 presents the temporal changes in electrical resistivity (ER) and induced polarization (IP) across the three test plots control (a–b), powdered WOS-amended (c–d), and granular WOS-amended (e–f) captured before (T_0) and after (T_9) the 9-month stabilization period. To ensure accurate interpretation of geophysical monitoring results, ER and IP tomograms were visualized using individually optimized color scales for each test plot. This approach was necessary because various site-specific factors such as differences in backfill density, soil heterogeneity, and moisture distribution may have influenced the absolute ER and IP values, potentially introducing visual or interpretational bias in cross-plot comparisons. Accordingly, the analysis focused on relative temporal changes within each plot, particularly within the 0–30 cm stabilization layer and its interface with the underlying contaminated soil. Temporal interpretations were further anchored to specific electrode positions coinciding with soil sampling locations, where ground-truth measurements (e.g., leaching ratios and heavy metal speciation) were independently validated. This integrated interpretation strategy allowed for the coupling of geophysical responses with subsurface geochemical dynamics over time.

In the control plot, the ER values in Fig. 6a span a wide range (50–5000 Ω·m), which may superficially suggest high heterogeneity in soil texture. Such localized high-resistivity zones shift or dissipate by T_9, suggesting that they are not fixed lithological features but may reflect transient zones of variable moisture retention or porosity. These changes could be attributed to seasonal water content redistribution (e.g., rainfall infiltration), differential drying, or compaction heterogeneity, rather than from by intrinsic changes in soil particle size[42]. The IP response (Fig. 6b) initially showed elevated chargeability (> 15 mV/V) across much of the upper 0.5 m, likely reflecting natural mineral surface polarization or weak clay-associated ionic retention[43]. After 9 months, while surface-level IP remained relatively stable, a distinct decline in chargeability was observed below 0.3 m depth, particularly in the right half of the plot (x = 1.5–2.5 m), where values dropped below 2 mV/V. Given the absence of any active intervention during this period, the cause of this localized decrease remains uncertain. One possible explanation is the downward redistribution of moisture due to gravitational drainage or capillary release during drying cycles, which could reduce ionic concentration in the lower unsaturated zone[44,45]. This may lead to dilution of charge carriers and a weakening of electrochemical double-layer polarization, thereby decreasing the IP response. Additionally, over time, local pore water may have approached chemical equilibrium with surrounding minerals, reducing ion exchange gradients and limiting surface polarization effects[46,47].

In the powdered amendment plot (Fig. 6c), the upper 0–30 cm zone is clearly distinguishable at T_0, with ER values ranging from 39 to 78 Ω·m substantially lower than those of the underlying untreated soil. This contrast is consistent with the introduction of WOS powder rich in calcium carbonate ($CaCO_3$), which readily dissolves under moist and mildly acidic to neutral soil conditions. Upon dissolution, $CaCO_3$ dissociates into Ca^{2+} and HCO_3^- ions, thereby increasing the ionic strength of the soil pore water[48]. The enhanced ionic concentration

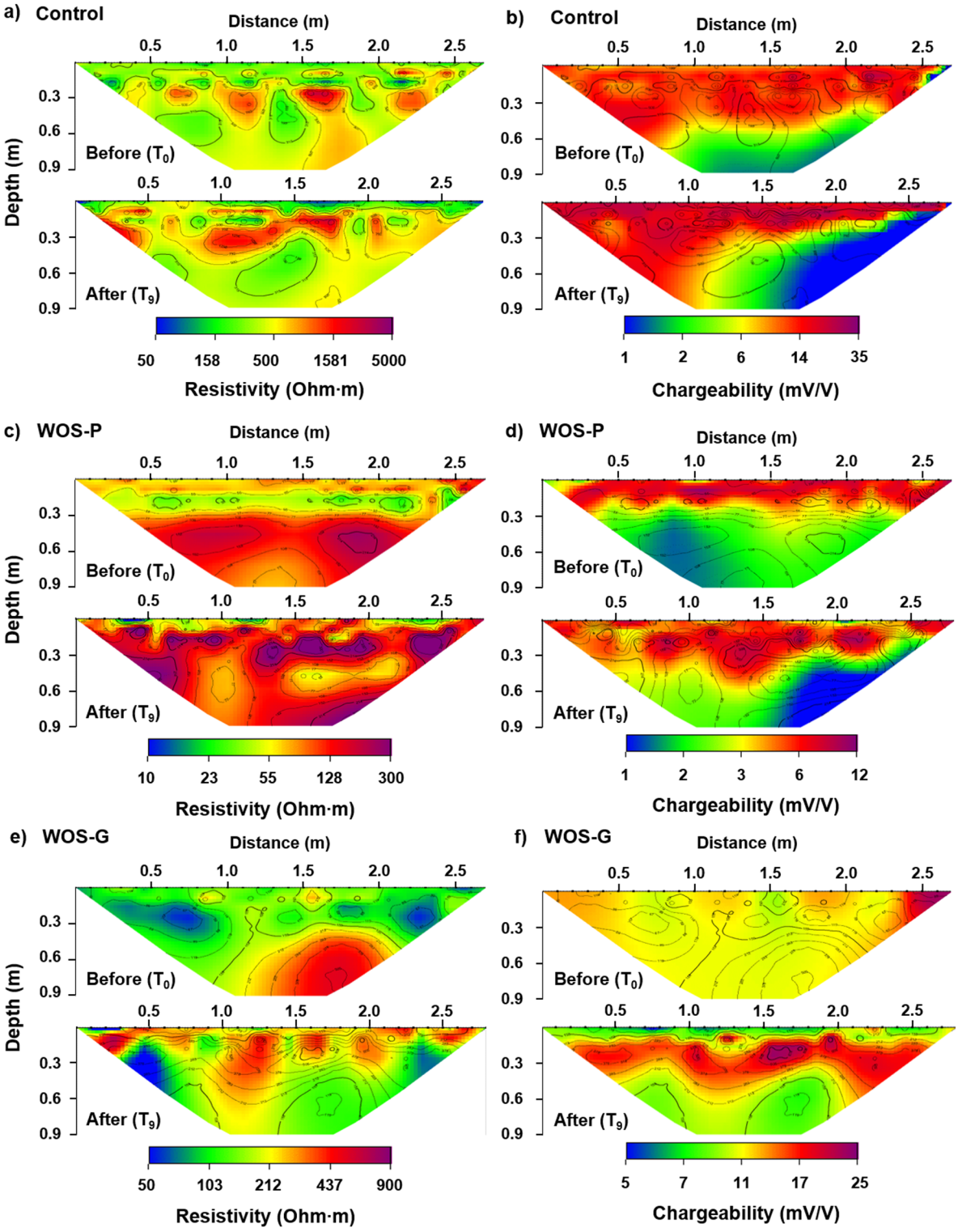

Fig. 6. ER and IP tomograms before (T_0) and after (T_9) stabilization in the three test plots: (a–b) Control (untreated), (c–d) WOS 5% (powder), and (e–f) WOS 5% (granular). Panels (a), (c), and (e) show resistivity distributions, while panels (b), (d), and (f) present chargeability distributions. The resistivity ranges are 50–5,000 Ω·m for the control plot, 10–300 Ω·m for the powdered WOS plot, and 50–900 Ω·m for the granular WOS plot. The corresponding chargeability ranges are 1–35 mV/V, 1–12 mV/V, and 5–25 mV/V, respectively. Color scales were independently optimized within each plot to visualize temporal changes between T_0 and T_9 rather than to standardize values across plots. Measurement depth extends from the surface to 90 cm, with horizontal lines marking the 30 cm stabilization layer in the amended plots.

reduces the bulk electrical resistivity of the soil by promoting more efficient charge transport through the pore space. Additionally, the dissolution of $CaCO_3$ leads to an increase in soil pH, which can further desorb exchangeable cations from mineral surfaces, contributing additional mobile ions to the pore solution[49]. These combined effects result in improved electrical conductivity and thus lower measured ER in the amended layer. Similarly, the IP signal in this plot (Fig. 6d) is elevated in the amended layer, particularly in the 20–30 cm range, where chargeability increases to 6–9 mV/V. This may be attributed to Ca^{2+} and HCO_3^- ions adsorbing onto soil mineral surfaces, enhancing interfacial polarization[50].

After 9 months, a significant shift is observed. ER values throughout the upper 0.3 m layer increase markedly, with values exceeding 200–400 Ω·m. This change is likely driven by the reduction of free ions through precipitation reactions such as the formation of carbonates, phosphates, or hydroxides under elevated pH conditions induced by $CaCO_3$ amendment[51,52]. As documented in prior work, prolonged $CaCO_3$ exposure leads to the formation of less conductive precipitates (e.g., $PbCO_3$), thereby increasing resistivity[53]. Concurrently, the depth of elevated IP response increases over time, which may reflect the progressive migration of mobile ions into deeper pore networks or the gradual chemical modification of mineral surface properties[54]. These processes can lead to more persistent electrochemical double-layer structures, enhancing interfacial polarization at greater depths. Such behavior is consistent with that of delayed precipitation or desorption-reabsorption cycles, especially under elevated pH conditions induced by $CaCO_3$ amendment[55].

Unlike the powdered form, the granular WOS-amended plot (Fig. 6e) did not show a clearly differentiated low-resistivity zone in the upper 30 cm at T_0. Instead, very low resistivity pockets (e.g., < 70 Ω·m) appear scattered near the center, likely caused by localized moisture accumulation or heterogeneities in backfill compaction. The lack of ER contrast suggests that the granular WOS did not dissolve significantly during early deployment and thus did not contribute markedly to pore fluid conductivity.

The IP pattern in Fig. 6f at T_0 was also subdued. However, by T_9, a marked increase in IP signal is observed near 30 cm depth, where chargeability rises from approximately 11 mV/V to nearly 25 mV/V in localized zones. This may reflect the delayed dissolution or surface weathering of granular WOS particles, releasing Ca^{2+} and carbonate species, thereby increasing the interfacial polarization over time. This delayed reactivity is supported by earlier studies showing time-dependent ion release from coarse $CaCO_3$ forms under field conditions[56].

The combined ER and IP monitoring suggests that powdered WOS amendment produces a rapid geophysical signature, characterized by lower ER and elevated IP, corresponding to the chemical mobility and ionic strength enhancement in the stabilized layer. Over time, this signature diminishes as ions precipitate or redistribute. Contrastingly, granular WOS does not initially modify the electrical properties significantly but shows increasing IP response with time, which is consistent with that of the delayed dissolution and ion release.

Thus, while ER is more useful for detecting powdered amendment shortly after application, IP emerges as the more robust monitoring tool for both amendment types over extended periods, particularly in evaluating ion-mediated stabilization behavior.

Conclusion

This study aimed to evaluate the stabilization efficiency of the WOS amendments WOS-P and WOS-G for Pb and Cu, and to assess the effectiveness of non-invasive geophysical methods for monitoring the process.

First, the results demonstrate that WOS is an effective amendment for immobilizing both metals, but that stabilization is achieved through distinct, element-specific mechanisms, with WOS-P showing superior performance. The application of WOS led to a marked reduction in the leaching ratios of Pb and Cu across all extraction methods. This stabilization effect was not only immediate but was also largely sustained over the 9-month monitoring period. Sequential extraction (Tessier) analysis provided strong chemical evidence explaining how this stability was achieved. The analysis confirmed that Pb and Cu were stabilized via different mechanisms. Pb was primarily stabilized through carbonate precipitation, whereas Cu was stabilized through adsorption onto Fe-Mn oxides. Second, the ER and IP results successfully demonstrated that geophysical methods can track stabilization processes in situ. ER provided a clear early indication of WOS-P application, while IP signals progressively intensified in both WOS types, reflecting ongoing mineral interactions. This highlights a key finding. While ER is advantageous for detecting immediate effects of fine-particle amendments, IP appears to be a more reliable long-term tool for assessing the ion-mediated stabilization dynamics that govern remediation success.

The primary contribution of this work, therefore, is the demonstration of an integrated geochemical-geophysical framework for monitoring the performance and mechanisms of in-situ stabilization. While the results are promising, several limitations frame the scope for future work. The 9-month monitoring period may not capture full seasonal variations, the study was conducted at a single site, and the absence of extended stability data limits the generalizability of these findings. Consequently, future research should prioritize multi-site, longer-term studies to validate long-term stability. Furthermore, there is a critical need for developing advanced interpretive frameworks that couple electrical signals with site-specific soil and contaminant behaviors. Such efforts will be essential for establishing cost-effective and time-efficient monitoring strategies tailored to diverse field conditions, ultimately enabling more accurate, adaptive, and scalable applications of ER and IP methods in long-term remediation assessment.

Data availability

The datasets used and/or analysed during the current study are available from the corresponding author on reasonable request.

Received: 29 June 2025; Accepted: 18 September 2025

Published online: 23 October 2025

References

1. Liu, L., Li, W., Song, W. & Guo, M. Remediation techniques for heavy metal-contaminated soils: principles and applicability. *Sci. Total Environ.* **633**, 206–219 (2018).
2. Yuksel, B. & Arica, E. Assessment of toxic, essential, and other metal levels by ICP-MS in lake Eymir and Mogan in Ankara, turkey: an environmental application. *At. Spectrosc.* **39**, 179–184 (2018).
3. Ahamad, M. I. et al. Contamination level, ecological risk, and source identification of heavy metals in the hyporheic zone of the Weihe River, China. *Int. J. Environ. Res. Public Health*. **17**, 1070 (2020).
4. Verma, S. & Kuila, A. Bioremediation of heavy metals by microbial process. *Environ. Technol. Innov.* **14**, 100369 (2019).
5. Ojuederie, O. B. & Babalola, O. O. Microbial and plant-assisted bioremediation of heavy metal polluted environments: a review. *Int. J. Environ. Res. Public Health*. **14**, 1504 (2017).
6. Spence, R. D. & Shi, C. *Stabilization and Solidification of Hazardous, Radioactive, and Mixed Wastes* (CRC, 2004).
7. Agency, U. S. E. P. *Treatment Technologies for Site Cleanup: Annual Status Report (Twelfth Edition). Report No. EPA 542-R-07-012* (U.S. Environmental Protection Agency, 2007).
8. Liu, J., Zha, F., Xu, L., Deng, Y. & Chu, C. in Proceedings of GeoShanghai 2018 International Conference: Geoenvironment and Geohazard. 442–449 (Springer).
9. Tian, Q. et al. Application of geopolymer in stabilization/solidification of hazardous pollutants: A review. *Molecules* **27**, 4570 (2022).
10. Li, Y., Jia, S. & Liu, J. Solidification, remediation and long-term stability of heavy metal contaminated soil under the background of sustainable development. *Sci. Rep.* **12**, 10330 (2022).
11. Kaludjerovic-Radoicic, T. & Raicevic, S. Aqueous Pb sorption by synthetic and natural apatite: Kinetics, equilibrium and thermodynamic studies. *Chem. Eng. J.* **160**, 503–510 (2010).
12. Hidmi, L. & Edwards, M. Role of temperature and pH in $Cu(OH)_2$ solubility. *Environ. Sci. Technol.* **33**, 2607–2610 (1999).
13. Choi, S. H. et al. Toward transformation of bivalve shell wastes into high value-added and sustainable products in South korea: A review. *J. Ind. Eng. Chem.* **129**, 38–52 (2024).
14. Saneiyan, S. et al. Induced polarization as a monitoring tool for in-situ microbial induced carbonate precipitation (MICP) processes. *Ecol. Eng.* **127**, 36–47 (2019).
15. Ahn, Y., Han, M. & Choi, J. Monitoring the mobility of heavy metals and risk assessment in mine-affected soils after stabilization. *J. Hazard. Mater.* **400**, 123231 (2020).
16. Moon, D. H. et al. Stabilization of As-, Pb-, and Cu-contaminated soil using calcined oyster shells and steel slag. *Environ. Sci. Pollut. Res.* **22**, 11162–11169 (2015).
17. Xu, D. M., Fu, R. B., Wang, J. X., Shi, Y. X. & Guo, X. P. Chemical stabilization remediation for heavy metals in contaminated soils on the latest decade: available stabilizing materials and associated evaluation methods-A critical review. *J. Clean. Prod.* **321**, 128730 (2021).
18. Yu, K. et al. Stabilization of heavy metals in soil using two organo-bentonites. *Chemosphere* **184**, 884–891 (2017).
19. Bagherifam, S., Lakzian, A., Fotovat, A., Khorasani, R. & Komarneni, S. In situ stabilization of as and Sb with naturally occurring Mn, al and Fe oxides in a calcareous soil: bioaccessibility, bioavailability and speciation studies. *J. Hazard. Mater.* **273**, 247–252 (2014).
20. Tessier, A., Campbell, P. G. & Bisson, M. Sequential extraction procedure for the speciation of particulate trace metals. *Anal. Chem.* **51**, 844–851 (1979).
21. Lee, S. J. et al. Development and validation of a statistical prediction model for estimating soil lead contamination in a sloped shooting range zone using geochemical and geophysical data. *J. Hazard. Mater. Adv.* **18**, 100760 (2025).
22. Martinho, E. Electrical resistivity and induced polarization methods for environmental investigations: an overview. *Water Air Soil. Poll.* **234**. https://doi.org/10.1007/s11270-023-06214-x (2023).
23. Kumar, P., Tiwari, P., Singh, A., Biswas, A. & Acharya, T. Electrical resistivity and induced polarization signatures to delineate the near-surface aquifers contaminated with seawater invasion in Digha, West-Bengal, India. *Catena* **207**, 105596 (2021).
24. Legislation, K. M. o. G (Korea Law Translation Center, Sejong, South Korea, 2019).
25. Wang, F., Li, W., Wang, H., Hu, Y. & Cheng, H. The leaching behavior of heavy metal from contaminated mining soil: the effect of rainfall conditions and the impact on surrounding agricultural lands. *Sci. Total Environ.* **914**, 169877 (2024).
26. Madadi, R., Kachoueiyan, F. & De-la-Torre, G. E. Effect of redox potential on the heavy metals binding phases in estuarine sediment: case study of the Musa estuary. *Mar. Pollut. Bull.* **195**, 115565 (2023).
27. Abdilla, B., Lee, S. S., Fenter, P. & Sturchio, N. C. Dynamic Inhibition of calcite dissolution in flowing acidic Pb2 + Solutions. *Environ. Sci. Technol.* **58**, 7133–7143 (2024).
28. Ok, Y. S., Lim, J. E. & Moon, D. H. Stabilization of Pb and cd contaminated soils and soil quality improvements using waste oyster shells. *Environ. Geochem. Health*. **33**, 83–91 (2011).
29. Feng, M. H., Shan, X. Q., Zhang, S. Z. & Wen, B. Comparison of a rhizosphere-based method with other one-step extraction methods for assessing the bioavailability of soil metals to wheat. *Chemosphere* **59**, 939–949 (2005).
30. Farshadirad, A., Hosseinpur, A. R., Motaghian, H. R. & Ghorbani Dashtaki, S. Zn fractionation and availability in different soil aggregate fractions from Isfahan region, central Iran. *Arch. Agron. Soil. Sci.* **63**, 1419–1430 (2017).
31. Yu, S., He, Z., Huang, C., Chen, G. & Calvert, D. Copper fractionation and extractability in two contaminated variable charge soils. *Geoderma* **123**, 163–175 (2004).
32. Zhang, Y., Zhang, L., Gao, R., Zhong, L. & Xue, J. CaCO3-coated PVA/BC-based composite for the simultaneous adsorption of Cu (II), cd (II), Pb (II) in aqueous solution. *Carbohydr. Polym.* **267**, 118227 (2021).
33. Xue, Z. F. et al. Investigating immobilization efficiency of Pb in solution and loess soil using bio-inspired carbonate precipitation. *Environ. Pollut*. **322**, 121218 (2023).
34. Mufalo, W. et al. Pilot-scale stabilization of toxic metal leachates from zinc plant residues using half-burnt dolomite: implications for remediation at Kabwe legacy mine in Zambia. *Environ. Geochem. Health*. **47**, 271 (2025).
35. Balint, R., Said-Pullicino, D. & Ajmone-Marsan, F. Copper dynamics under alternating redox conditions is influenced by soil properties and contamination source. *J. Contam. Hydrol.* **173**, 83–91 (2015).
36. Ishigami, D. et al. Utilization of the finer particle fraction of arsenic-bearing excavated rock mixed with iron-based adsorbent as sorption layer. *Minerals* (2075-163X) 15 (2025).
37. Kajiyoshi, M. et al. Long-term performance of the adsorption layer system for the recycling and repurposing of arsenic-bearing mudstone as road embankment. *Chemosphere* **363**, 142985 (2024).
38. Cui, H. et al. Combined application of ferrihydrite and hydroxyapatite to immobilize soil copper, cadmium, and phosphate under flooding-drainage alternations. *Environ. Pollut*. **292**, 118323 (2022).
39. Demangeat, E. et al. Surface modifications at the oxide/water interface: implications for Cu binding, solution chemistry and chemical stability of iron oxide nanoparticles. *Environ. Pollut*. **257**, 113626 (2020).
40. Sipos, P., Németh, T., Kis, V. K. & Mohai, I. Sorption of copper, zinc and lead on soil mineral phases. *Chemosphere* **73**, 461–469 (2008).
41. Alghamdi, A. G. & Alasmary, Z. Fate and transport of lead and copper in calcareous soil. *Sustainability* **15**, 775 (2022).

42. Zhang, G. et al. Imaging rainfall infiltration processes with the time-lapse electrical resistivity imaging method. *Pure. appl. Geophys.* **173**, 2227–2239 (2016).
43. Slater, L., Ntarlagiannis, D. & Wishart, D. On the relationship between induced polarization and surface area in metal-sand and clay-sand mixtures. *Geophysics* **71**, A1–A5 (2006).
44. Lessoff, S. & Indelman, P. Analytical model of solute transport by unsteady unsaturated gravitational infiltration. *J. Contam. Hydrol.* **72**, 85–107 (2004).
45. Aldrees, A. & Nachabe, M. Capillary length and field capacity in draining soil profiles. *Water Resour. Res.* **55**, 4499–4507 (2019).
46. Slater, L. D. & Lesmes, D. IP interpretation in environmental investigations. *Geophysics* **67**, 77–88 (2002).
47. Lesmes, D. P. & Frye, K. M. Influence of pore fluid chemistry on the complex conductivity and induced polarization responses of berea sandstone. *J. Geophys. Research: Solid Earth*. **106**, 4079–4090 (2001).
48. Peker, A. E., Öztürk, H. S. & Mamedov, A. I. The effect of sodic water type on the chemical properties of calcareous soil in Semi-Arid irrigated land. *Soil. Syst.* **8**, 10 (2024).
49. Goren, O., Gavrieli, I., Burg, A. & Lazar, B. Cation exchange and CaCO3 dissolution during artificial recharge of effluent to a calcareous sandstone aquifer. *J. Hydrol.* **400**, 165–175 (2011).
50. Gao, X. et al. Specific ion effects: the role of anions in the aggregation of permanently charged clay mineral particles. *J. Soils Sediments*. **23**, 263–272 (2023).
51. Tamir, G. et al. Organic N mineralization and transformations in soils treated with animal waste in relation to carbonate dissolution and precipitation. *Geoderma* **209**, 50–56 (2013).
52. Yu, X., Keitel, C. & Dijkstra, F. A. Ameliorating soil acidity with calcium carbonate and calcium hydroxide: effects on carbon, nitrogen, and phosphorus dynamics. *J. Soil. Sci. Plant. Nutr.* **23**, 5270–5278 (2023).
53. Zha, F. et al. Electrical resistivity evaluation of MICP solidified lead contaminated soil. *Environ. Earth Sci.* **83**, 261 (2024).
54. Schwartz, N. & Furman, A. Spectral induced polarization signature of soil contaminated by organic pollutant: experiment and modeling. *J. Geophys. Research: Solid Earth* **117** (2012).
55. Du, W. et al. Specific ion effects of incomplete ion-exchange by electric field-induced ion polarization. *RSC Adv.* **10**, 15190–15198 (2020).
56. Zhu, T. & Dittrich, M. Carbonate precipitation through microbial activities in natural environment, and their potential in biotechnology: a review. *Front. Bioeng. Biotechnol.* **4**, 4 (2016).

Acknowledgements

We would like to thank Editage (www.editage.co.kr) for English language editing.

Author contributions

S.J.L. collected and analyzed the data, contributed to the conceptualization of the study, and drafted the manuscript. M.J.K. contributed to data collection. N.R.L. contributed to the preparation of figures. Y.T.A. contributed to the conceptualization of the study and reviewed and revised the manuscript. J.Y.C. designed the study, supervised the research, and critically reviewed and revised the manuscript. All authors reviewed and approved the final manuscript.

Funding

This research is supported by the Korea Environment Industry & Technology Institute (KEITI) through the Subsurface Environmental Pollution Risk Management Technology Development Project, funded by the Korea Ministry of Environment (MOE)(RS-2023-00220588).

Declarations

Competing interests

The authors declare no competing interests.

Additional information

Correspondence and requests for materials should be addressed to J.C.

Reprints and permissions information is available at www.nature.com/reprints.

Publisher's note Springer Nature remains neutral with regard to jurisdictional claims in published maps and institutional affiliations.

Open Access This article is licensed under a Creative Commons Attribution-NonCommercial-NoDerivatives 4.0 International License, which permits any non-commercial use, sharing, distribution and reproduction in any medium or format, as long as you give appropriate credit to the original author(s) and the source, provide a link to the Creative Commons licence, and indicate if you modified the licensed material. You do not have permission under this licence to share adapted material derived from this article or parts of it. The images or other third party material in this article are included in the article's Creative Commons licence, unless indicated otherwise in a credit line to the material. If material is not included in the article's Creative Commons licence and your intended use is not permitted by statutory regulation or exceeds the permitted use, you will need to obtain permission directly from the copyright holder. To view a copy of this licence, visit http://creativecommons.org/licenses/by-nc-nd/4.0/.

© The Author(s) 2025